Dynamics of Individual Single-Walled Carbon Nanotubes in Water by Real-Time Visualization

Rajat Duggal and Matteo Pasquali*

Department of Chemical and Biomolecular Engineering, Department of Chemistry, Carbon Nanotechnology Laboratory, Center for Biological and Environmental Nanotechnology, The Smalley Institute for Nanoscale Science and Technology, Rice University, Houston, Texas 77005, USA

(Received 13 December 2005; published 23 June 2006)

Individual single-walled carbon nanotubes (SWNTs) in aqueous suspension are visualized directly by fluorescence video microscopy. The fluorescent tagging is simple, biocompatible, and does not modify the SWNTs. The dynamics of individual SWNTs in water are observed and quantified for the first time. We measure the confined rotational diffusion coefficient and find it in reasonable agreement with predictions based on confined diffusion of dilute Brownian rods. We determine the critical concentration at which SWNTs in suspensions start interacting. By analyzing the fluctuating shape of SWNTs in the 3 to 5 μm range, we determine that their persistence length ranges between 32 and 174 μm, in agreement with theoretical estimates; thus, commonly available SWNTs in liquids can be considered as rigid Brownian rods in the absence of imposed external fields or self-attractive forces.

DOI: 10.1103/PhysRevLett.96.246104 PACS numbers: 81.07.De, 82.70.Kj, 83.85.Ei

The behavior of single-walled carbon nanotubes (SWNTs) in liquids is still poorly understood. This is perhaps surprising, because SWNTs are commonly described as high aspect ratio rodlike particles, and slender rigid objects in liquids have been studied for decades [1–3]. The difficulty in dispersing SWNTs in liquids and the lack of viable techniques for observing their dynamics in suspensions have slowed fundamental progress on liquid-phase behavior of SWNTs. SWNTs in liquids are important in the physical, material, and life sciences; real-time visualization of SWNTs in liquids can impact each of these areas of research. Liquid-phase processing is key to developing scalable techniques for directed assembly or self-assembly of SWNTs, e.g., production of SWNT fibers [4] and films [5], length and type separation of SWNTs. The high aspect ratio and stiffness of SWNTs may enable more efficient delivery of genes and drugs through cell membranes [6]; directly visualizing SWNTs in water would yield detailed information on the interaction of SWNTs with cells [6,7] and biomolecules—DNA and proteins can provide unique and selective building blocks for directed assembly of SWNTs into functional nanoscale and microscale structures, e.g., sensors [8]. Visualization can also be important for controlled manipulation of SWNTs into nanostructures, e.g., by optical trapping and tweezing [9]. From a fundamental viewpoint, it is not known whether the theoretical predictions of rotational diffusivity and persistence length stemming from the assumption that SWNTs are homogeneous hollow cylinders [10,11] can be applied to SWNTs in liquids because the diameter of a SWNT ($\sim$1 nm) is close to the size of the solvent molecules, and any imperfections in the sidewalls of the nanotubes could affect dynamic properties. High resolution techniques like transmission electron microscopy and atomic force microscopy yield SWNT length and diameter [12,13], but do not provide real-time dynamics in liquids and cannot be applied to living systems. The dynamics of small objects, including SWNTs, in liquids have been studied using bulk techniques such as light and neutron scattering [14,15] and birefringence [16]; these techniques involve large ensembles of molecules and the interpretation of results is difficult when samples are poorly characterized and polydisperse, as is always the case with SWNTs. These difficulties hinder greatly progress on characterization and certification of SWNT samples, posing problems both to producers and users; direct determination of SWNT rotational and bending properties in liquids would remove these barriers to widespread commercial use. Single molecule fluorescence video microscopy has provided dynamic information on molecules and small particles like F-actin [17], microtubules [17], DNA [18,19], and wormlike micelles [20]. Recent progress has been reported on fluorescence visualization of SWNTs [6,21–25]; the most promising method developed so far relies on the spontaneous infrared fluorescence of SWNTs [25]. These techniques do not have sufficient temporal and spatial resolution to yield the dynamics of SWNTs in liquids. Here we present a simple and convenient SWNT fluorescent tagging procedure; with this technique, we study the dynamics of individual SWNTs in water by video microscopy.

As-synthesised SWNTs exist as bundles or aggregates bound tightly by strong van der Waals forces. The SWNTs were dispersed as individuals in an aqueous solution of sodium dodecyl sulphate (SDS) [12]. In water, SDS above the critical micelle concentration (8.1 mM) exists as spherical micelles up to a concentration of 810 mM [26]. During sonication in water with SDS, individual SWNTs get encased in SDS micelles [Fig. 1(a)] whose estimated diameter is $\sim$7 nm [27]. Raman and fluorescence spectroscopy [12,27] of the dispersion showed that the SWNTs in solution were dispersed individually (Fig. S1 in Ref. [28]). The first moment and cube root of the third moment of the length distribution in the polydisperse sample were $\langle L \rangle \approx 250$ nm and $\langle L^3 \rangle^{1/3} \approx 440$ nm (determined by atomic

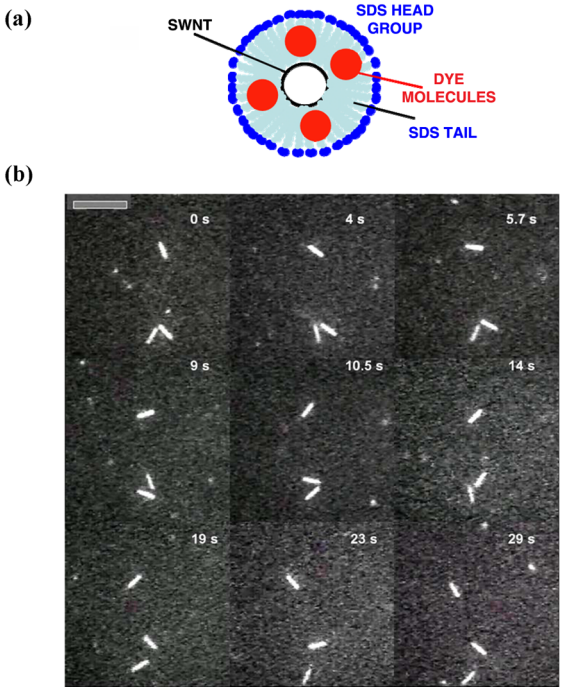

FIG. 1 (color online). Fluorescence visualization of individual SWNTs. (a) Schematic of the SWNT-SDS-Dye complex. The surfactant hydrocarbon chains arrange on the surface of the encapsulated SWNT. Spheres represent dye molecules. (b) Time lapse images of diffusing SWNTs. Scale bar is 10 μm.

force microscopy and dilute solution rheology [29]). The SDS-SWNT complexes were labeled with a hydrophobic red fluorescent dye PKH26 [28] which was added to the aqueous suspension and incorporated spontaneously into the core of the micelles. Adding the dye did not affect the Raman and fluorescence spectra; thus, the SWNTs did not aggregate when the dye was added. Figure 1(b) shows images of fluorescent individual SWNTs undergoing Brownian motion. Diffraction limited the resolution of SWNT diameters; however, SWNTs longer than about 1 μm were readily identified and visualized in focus for tens of seconds or longer (movie1.wmv in Ref. [28]). This simple fluorescent tagging technique can be used with other surfactant-nanotube systems (e.g., pluronics). Visualization of control samples of surfactants and dye without SWNTs showed only diffuse fluorescence and lacked any identifiable slender objects.

Rotational diffusion of an ensemble of Brownian rigid rods is described by the Debye equation [10,30]. In spherical coordinates the solution of this diffusion equation can be expressed conveniently in terms of a set of orthogonal eigenfunctions [10]—spherical harmonics, a combination of trigonometric functions and Legendre polynomials $P_k(x)$. The autocorrelation of the two-dimensional projection $\mathbf{u}(t)$ of the fluctuating orientation of rods in the ensemble decays exponentially in time; the correlation functions are described by

$$\langle P_k(\mathbf{u}(t)\cdot\mathbf{u}(0))\rangle = \exp(-D_k^R k(k+1)/2t)$$

where D_k^R are the diffusion coefficients (rates of decay) of the different harmonics. A suspension of rods is considered dilute if each rod can rotate freely without being affected by other rods; in this case, all diffusion coefficients are equal ($D_k^R = D^R$) and independent of rod concentration [30]. The transition to the semidilute regime, where rod-rod interactions become important, occurs when the number concentration υ reaches a value proportional to L^{-3}, where L is the length of the rods. Theory predicts that in monodisperse samples the transition should occur at $\upsilon^* = 1/\langle L^3\rangle$; bulk measurements on polydisperse samples show that the transition occurs at $\upsilon \approx 30/\langle L^3\rangle$ [11]. We prepared solutions at number concentrations $2\upsilon^*$ and $0.3\upsilon^*$ [28] and measured the decay of the orientational correlation functions. Figure 2 (insets) shows that the orientational correlation functions decay exponentially at both concentrations. At $0.3\upsilon^*$ [Fig. 2(a)], the first three harmonics of a 3.3 ± 0.2 μm SWNT decay at the same rate, indicating that the SWNT is in a dilute suspension. At the higher concentration [Fig. 2(b)], the decay rates of the first three harmonics of a 3.4 ± 0.3 μm SWNT are different, i.e., this SWNT is interacting with others. Figure 2 shows the ratio of the second and third diffusion coefficients with respect to the first, measured on 27 SWNTs at the two concentrations. At the lower concentration $\langle D_2^R/D_1^R\rangle = 0.95 \pm 0.04$ ($\langle D_3^R/D_1^R\rangle = 0.90 \pm 0.08$); i.e., the diffusion coefficients D_k^R are equal and the suspension is dilute. At the higher concentration $\langle D_2^R/D_1^R\rangle = 0.91 \pm 0.14$

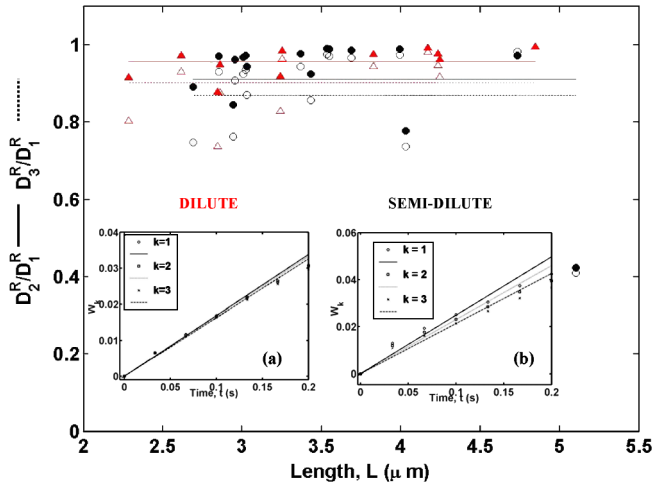

FIG. 2 (color online). Dilute to semidilute transition. Ratio of the second D_2^R (filled symbols) and third D_3^R (open symbols) two-dimensional rotational diffusivities with respect to the first D_1^R, at concentration $2\upsilon^*$ (black ○) and $0.3\upsilon^*$ [△ (red online)]. Lines indicate average values (solid line D_2^R/D_1^R and dashed line D_3^R/D_1^R). Insets: (a) The orientation correlation functions overlap at the lower concentration; thus, this 3.3 ± 0.2 μm SWNT is noninteracting at $0.3\upsilon^*$. (b) The orientation correlation functions do not overlap at the higher concentration; thus, this 3.4 ± 0.3 μm SWNT is interacting at $2\upsilon^*$. Times below 0.15 s were used to fit $W_k = -\frac{2}{k(k+1)}\ln\langle P_k(\mathbf{u}(t)\cdot\mathbf{u}(0))\rangle$; $P_1(x) = x$; $P_2(x) = 1.5x^2 - 0.5$; $P_3 = 2.5x^3 - 1.5x$.

($\langle D_3^R/D_1^R\rangle = 0.87 \pm 0.15$) and the suspension is transitioning to semidilute.

Figure 3 shows the measured two-dimensional rotational diffusivity as a function of SWNT length. The measured diffusivity is lower than that predicted theoretically for noninteracting rigid rods in bulk (solid line in Fig. 3) [10,31]. Here the nanotubes are confined between two glass plates separated by a small gap (~2.5 μm, Fig. 3 inset); thus, wall effects (which slow down diffusion) must be considered. Superposing the drag on a rod due to the two walls gives the confined rotational diffusion coefficient [32]. The measured diffusivity is about 40% below that predicted by the confinement model (Fig. 3), which is reasonable agreement within the scatter of the data.

The stiffness of an inextensible elastic threadlike object is characterized by its bending stiffness κ [33]. When a microscopic thread is placed in a liquid, the balance between Brownian forces, which tend to bend the thread, and elastic forces, which oppose curvature, is characterized by the persistence length $L_p = \kappa/k_BT$ (k_B is the Boltzmann constant)—the contour distance along the thread over which the tangent to the thread contour remains correlated, in the absence of flow and other forces [11]. The literature is divided on whether, in the absence of flow, individual SWNTs in liquids should be considered rigid ($L_p \gg L$) or semiflexible ($L_p \sim L$): theoretical estimates [34] based on measurements of bending stiffness [35] predict persistence length of tens of micrometers; experiments based on the size of closed SWNT rings [36] estimated the persistence length to 800 nm; recent neutron scattering data [15] show that SWNTs behave as rigid rods on length scales of at least ~150 nm, whereas earlier x-ray scattering [37] indicated that SWNT do not display rodlike behavior at any length. The persistence length can be determined through the bending stiffness, which can be measured from the response (deflection) of a thread to an imposed force [35], although this is arduous at the nanoscale because of the intrinsic difficulties in precisely imposing forces on and measuring deflection of individual SWNTs. Intrinsic thermal vibrations in vacuum also induce undulations and can be used to measure SWNT stiffness [38]. The shape (local tangent angle) of an elastic thread can be expressed conveniently as a sum of bending modes (biharmonic functions) of increasing wave number; in the absence of external forces, equipartition of energy dictates that the variance of the amplitude of the bending modes of a thread immersed in a liquid is inversely proportional to the product of the persistence length and the wave number squared. Thus, the persistence length can be determined by measuring the distribution of amplitudes of bending modes from images of a SWNT undergoing thermal undulation in water.

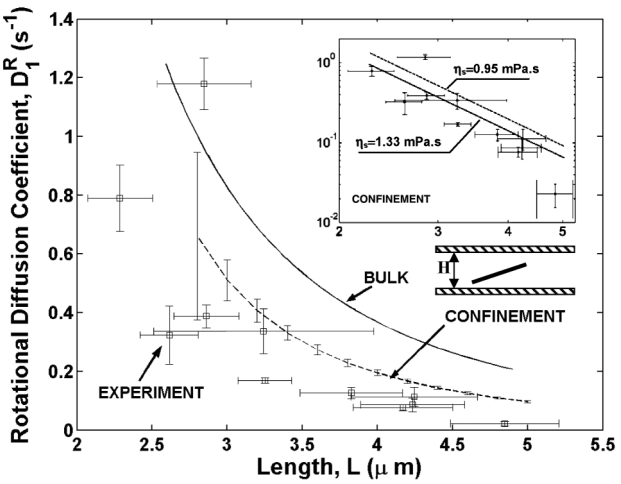

FIG. 3. Two-dimensional rotational diffusivity D_1^R of SWNTs as a function of length at concentration $0.3v^*$. Symbols are the experimental measurements. The solid line is prediction in bulk [31] $D^R = \frac{3k_BT(\ln(\frac{L}{b})-\gamma)}{\pi\eta_s L^3}$ (diameter $b = 7$ nm, solvent viscosity $\eta_s = 0.95$ mPa s, $\gamma \approx -0.446$). The broken line is the average diffusivity in a two-dimensional confined geometry (plate separation 2.5 ± 0.3 μm) computed through Eq. 5 of Ref. [32]. Error bars are standard deviation of the length and the errors in the linear fits. Inset: The best-fit line of the confinement model (solid line) is obtained by assuming a fluid viscosity ~40% higher than measured.

Nanotube images for shape analysis were acquired at time intervals of 333 ms to ensure that they were uncorrelated (the first bending mode of rods of length <4 μm and $L_p \sim 20$ μm relaxes in $\tau_b \approx \frac{4\pi\eta L^4}{500k_BTL_p\ln(L/d)} < 10$ ms). Images were thresholded and reduced to a single pixel backbone by standard image processing (Matlab skeletonization). Using the procedure of Gittes *et al.* [17], the shape of the backbone was expressed as a sum of ten Fourier modes (n) $\theta(s) = \sqrt{2/L}\sum_{n=0}^{10} a_n \cos(n\pi s/L)$, where $\theta(s)$ is the tangent angle along the arc s of the rod with contour length L. The variance of the distribution of mode amplitudes $\langle a_n^2\rangle$ was corrected to account for noise due to limited resolution of the imaging system [17] and the persistence length was calculated as $L_p^{-1} = (n\pi/L)^2 \times [\langle a_n^2\rangle^{\text{measured}} - \langle a_n^2\rangle^{\text{noise}}]$. Measurements of persistence length were restricted to 13 nanotubes with length greater than 3 μm because images of shorter nanotubes did not show sufficient bending. As expected [17], in short, stiff filaments, experimental noise dominated the thermal fluctuations in the higher modes; hence, the measurements from the higher modes are not reported. Because all experiments were performed at the same ionic strength, they combine the effects of the intrinsic and electrostatic persistence length (the electrostatic effect should be minimal because the Debye screening length is about 1.7 nm).

Figure 4 shows the persistence length of 13 nanotubes measured using the first bending mode: the measured values range from 32 μm to 174 μm. Based on the in-plane stiffness calculated using density functional theory [39] ($C = 345$ N/m) and its relationship to the bending stiffness $\kappa = \pi CR^3$, the persistence length of HiPco SWNTs (typical [40] radius R to 0.3 to 0.65 nm) is estimated [34] to be ~7 to 74 μm, which is consistent with the

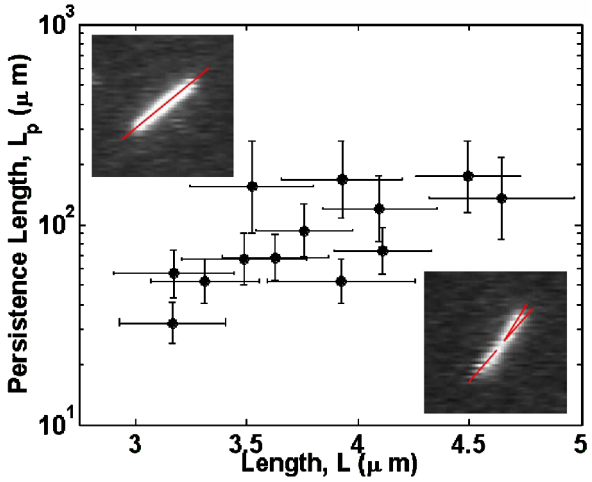

FIG. 4 (color online). Persistence length L_p of SWNTs of different lengths determined by the amplitude of the first Fourier mode ($n = 1$) describing their shapes. About 100 images of each SWNT were used to measure the distribution of mode amplitudes. The error in the contour length is the standard deviation and the error in the persistence length is computed by Eq. 23 of Ref. [17]. Inset: An almost straight (top left) and a bent (bottom right) configurations of the same SWNT (length 3.6 μm, persistence length 68.5 μm).

experimental results in Fig. 4. Most SWNTs samples comprise SWNTs shorter than 1 μm; clearly $L_p \gg L$ and single-walled carbon nanotubes in liquid can be considered as rigid in the absence of imposed external fields (e.g., flow) or self-attractive forces.

We have presented a simple and convenient fluorescent tagging procedure for visualizing in real time individual surfactant-stabilized SWNTs in water by standard visible-light microscopy. By using this method, we provide the first data on SWNT rotational diffusion coefficient and show that the measurements agree with predictions based on the theory of confined diffusion of slender Brownian rods. We report the first direct measurements of SWNT persistence length in a liquid; in the range of our measurements (SWNTs 3 to 5 μm long), we show that they agree with theoretical estimates. This new visualization method will be invaluable for understanding the dynamics of nanotubes in suspension, e.g., in sorting of nanotubes by flow-fractionation, electrophoresis, in making aligned films and fibers by liquid processing methods, and in studying the interaction of nanotubes with living organisms (e.g., cells) and biological molecules like DNA.

We thank R. E. Smalley and R. H. Hauge for providing SWNTs, N. Parra-Vasquez for SWNT dispersions, M. Provenzano and N. Fakri for image acquisition and analysis, and F. Hussain, A. Montesi, R. B. Weisman, D. A. Tsyboulski, Y. Wang, H. K. Schmidt, V. C. Moore, and P. Cherukuri for discussions. This work was supported by NSF CTS-CAREER 0134389 and the NSF Center for Biological and Environmental nanotechnology (EEC-0118007).

*To whom correspondence and requests for materials should be addressed.
Email address: mp@rice.edu

[1] G. B. Jeffery, Proc. R. Soc. A **102**, 161 (1922).
[2] J. G. Kirkwood, *Macromolecules* (Gordon and Breach, New York, 1967).
[3] L. Onsager, Ann. N.Y. Acad. Sci. **51**, 627 (1949).
[4] B. Vigolo *et al.*, Science **290**, 1331 (2000).
[5] Z. Wu *et al.*, Science **305**, 1273 (2004).
[6] Q. Lu *et al.*, J. Appl. Phys. **96**, 6772 (2004).
[7] P. Cherukuri *et al.*, J. Am. Chem. Soc. **126**, 15 638 (2004).
[8] Y. Lin *et al.*, J. Mater. Chem. **14**, 527 (2004).
[9] J. Plewa *et al.*, Opt. Express **12**, 1978 (2004).
[10] M. Doi and S. F. Edwards, *The Theory of Polymer Dynamics* (Oxford Press, New York, 1986).
[11] R. G. Larson, *The Structure and Rheology of Complex Fluids* (Oxford Press, New York, 1999).
[12] V. C. Moore *et al.*, Nano Lett. **3**, 1379 (2003).
[13] C. Richard *et al.*, Science **300**, 775 (2003).
[14] S. Badaire *et al.*, Langmuir **20**, 10 367 (2004).
[15] W. Zhou *et al.*, Chem. Phys. Lett. **384**, 185 (2004).
[16] J. F. Maguire, J. P. McTague, and F. Rondelez, Phys. Rev. Lett. **45**, 1891 (1980).
[17] F. Gittes *et al.*, J. Cell Biol. **120**, 923 (1993).
[18] S. B. Smith, L. Finzi, and C. Bustamante, Science **258**, 1122 (1992).
[19] T. T. Perkins *et al.*, Science **264**, 822 (1994).
[20] P. Dalhaimer, F. S. Bates, and D. E. Discher, Macromolecules **36**, 6873 (2003).
[21] K. Otobe *et al.*, Nano Lett. **2**, 1157 (2002).
[22] R. Rao *et al.*, Appl. Phys. Lett. **85**, 4228 (2004).
[23] S. Chaudhary *et al.*, Nano Lett. **4**, 2415 (2004).
[24] R. Prakash *et al.*, Appl. Phys. Lett. **83**, 1219 (2003).
[25] D. A. Tsyboulski, S. M. Bachilo, and R. B. Weisman, Nano Lett. **5**, 975 (2005).
[26] H. Shirota, Y. Tamoto, and H. Segawa, J. Phys. Chem. A **108**, 3244 (2004).
[27] M. J. O'Connell *et al.*, Science **297**, 593 (2002).
[28] See EPAPS Document No. E-PRLTAO-96-038625 for materials and methods, data analysis, and a movie showing rotational diffusion of a SWNT. For more information on EPAPS, see http://www.aip.org/pubservs/epaps.html.
[29] A. N. G. Parra-Vasquez *et al.* (to be published).
[30] T. Kirchhoff, H. Lowen, and R. Klein, Phys. Rev. E **53**, 5011 (1996).
[31] S. Broersma, J. Chem. Phys. **74**, 6989 (1981).
[32] G. Li and J. X. Tang, Phys. Rev. E **69**, 061921 (2004).
[33] E. M. Lifshitz and L. V. Landau, *Theory of Elasticity* (Butterworth-Heinemann, Oxford, 1980).
[34] B. I. Yakobson and L. S. Couchman, in *Dekker Encyclopedia of Nanoscience and Nanotechnology*, edited by J. A. Schwarz, C. I. Contescu, and K. Putyera (Marcel Dekker, Inc., New York, 2004), pp. 587.
[35] J. Salvetat *et al.*, Phys. Rev. Lett. **82**, 944 (1999).
[36] M. Sano *et al.*, Science **293**, 1299 (2001).
[37] D. W. Schaefer *et al.*, Chem. Phys. Lett. **375**, 369 (2003).
[38] M. M. J. Treacy, T. W. Ebbesen, and J. M. Gibson, Nature (London) **381**, 678 (1996).
[39] K. N. Kudin, G. E. Scuseria, and B. I. Yakobson, Phys. Rev. B **64**, 235406 (2001).
[40] S. M. Bachilo *et al.*, Science **298**, 2361 (2002).